

Anyview: Generalizable Indoor 3D Object Detection with Variable Frames

Zhenyu Wu¹, Xiuwei Xu², Ziwei Wang², Chong Xia², Linqing Zhao³, Jiwen Lu² and Haibin Yan^{*1}

Abstract—In this paper, we propose a novel network framework for indoor 3D object detection to handle variable input frame numbers in practical scenarios. Existing methods only consider fixed frames of input data for a single detector, such as monocular RGB-D images or point clouds reconstructed from dense multi-view RGB-D images. While in practical application scenes such as robot navigation and manipulation, the raw input to the 3D detectors is the RGB-D images with variable frame numbers instead of the reconstructed scene point cloud. However, the previous approaches can only handle fixed frame input data and have poor performance with variable frame input. In order to facilitate 3D object detection methods suitable for practical tasks, we present a novel 3D detection framework named AnyView for our practical applications, which generalizes well across different numbers of input frames with a single model. To be specific, we propose a geometric learner to mine the local geometric features of each input RGB-D image frame and implement local-global feature interaction through a designed spatial mixture module. Meanwhile, we further utilize a dynamic token strategy to adaptively adjust the number of extracted features for each frame, which ensures consistent global feature density and further enhances the generalization after fusion. Extensive experiments on the ScanNet dataset show our method achieves both great generalizability and high detection accuracy with a simple and clean architecture containing a similar amount of parameters with the baselines.

Index Terms—3D object detection, generalizability.

I. INTRODUCTION

3D object detection is a fundamental scene understanding problem for robotic manipulation [45], [57], autonomous driving [46], and AR/VR [54], [27], which aims to detect the 3D bounding boxes and semantic labels from point clouds or images. Due to the different types of sensors used in different application scenarios, 3D object detection methods usually vary a lot for indoor [33], [13] and outdoor [61] scenes. We focus on indoor 3D object detection, where the mainstream sensor is RGB-D cameras and the scenes are crowded with objects of multiple categories and sizes.

Although great improvement in performance has been achieved by advanced architecture design, existing methods

*Corresponding author.

¹Zhenyu Wu and Haibin Yan are with the School of Automation, Beijing University of Posts and Telecommunications, Beijing, 100876, China. {wuzhenyu, eyanhaibin}@bupt.edu.cn.

²Xiuwei Xu, Ziwei Wang, Chong Xia, and Jiwen Lu are with the Department of Automation, Tsinghua University, and Beijing National Research Center for Information Science and Technology (BNRist), Beijing, 100084, China. {xxw21, wang-zw18, xiact20}@mails.tsinghua.edu.cn. lujiwen@tsinghua.edu.cn.

³Linqing Zhao is with the School of Electrical and Information Engineering, Tianjin University, Tianjin, 300072, China. {linqingzhao}@tju.edu.cn

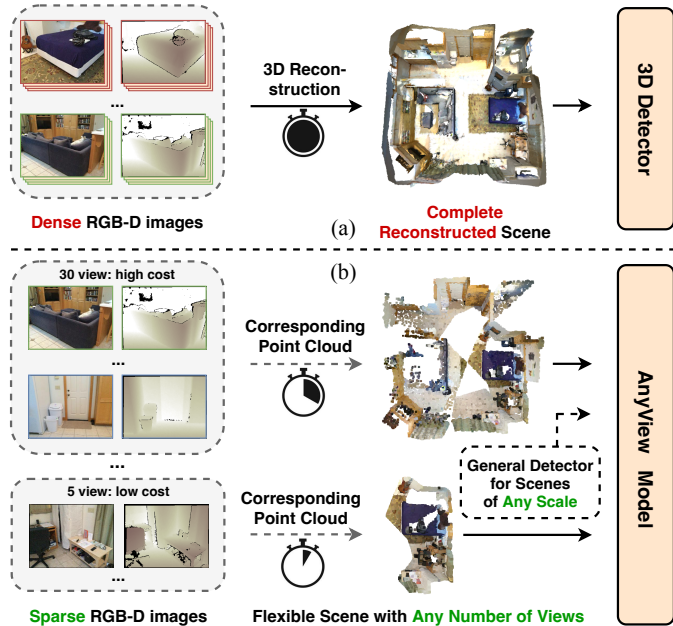


Fig. 1. (a) Previous 3D object detection methods rely on reconstructed point clouds from densely sampled RGB-D images, which requires a large amount of time to process the data and generalizes poorly to scenes in different scales. (b) Our method directly detects objects from sparse RGB-D images of any number of views, which shows good generalizability and provides more trade-off.

train and evaluate 3D detectors on only fixed frames of input data, such as monocular RGB-D images (on SUN-RGBD [37] benchmark) and scene-level reconstructed point clouds (sampled from meshes) from multi-view RGB-D images (on ScanNet [5] benchmark). There is still a huge gap between these benchmarks and practical applications. Specifically, due to the various task budgets in practical application scenes, the number of frames input to the 3D detectors is dynamic, and previous frameworks trained on fixed frame inputs are challenging to generalize. The cost of training diverse models for tasks with various sizes of inputs is huge, severely limiting the deployment of the models on edge devices. In order to solve this problem, it is necessary to further research and develop more efficient generalized indoor 3D object detection with variable frames. For example, in online tasks such as robot navigation [12], [49], [18], the information captured by the agent is strictly limited by a cost budget constraint, which leads to a varying number of input frames. As we will show in Section III-A, previous models generalize poorly across different input scales, which brings a huge burden as we need to prepare a series of models trained on different scales of input data to cope with various scenarios.

In practical scenes, the raw input to the indoor 3D object

detectors is the RGB-D images with variable frame numbers. The detectors require the ability to process inputs with various frame numbers at fixed parameters to complete different tasks. To simulate this, we propose a novel processing framework named AnyView for indoor 3D object detection as shown in Fig. 1. Previous approaches require a complete reconstruction of the scene point cloud through dense RGB-D images before input. This limitation results in the models only being able to process a fixed frame number of RGB-D image inputs, leading to weak generalization. In addition, a large amount of resources are wasted in the scene reconstruction process. Compared with previous approaches, our proposed AnyView can handle variable frame numbers of input data to satisfy the cost budgets of various practical applications. Specifically, we first unify the modality of input data as sparse multi-view RGB-D images and the corresponding camera parameters, which are compatible with current benchmark datasets (e.g. ScanNet [5] and SUN-RGBD [37]). Instead of concatenating multi-view point clouds into a whole and extracting a fixed number of global features of scenes, we learn geometric clues for each frame independently and design a transformer-based architecture to merge and refine the extracted features of various frames to achieve the ability to efficiently process variable frame inputs. Specifically, we propose a geometric learner to mine local geometric structural features and employ a spatial mixtures module to fuse local details with global semantics. In this way, AnyView is able to extract rich representations for input scenes consisting of any number of frames, bridging the gap between the local geometric features of each frame and the global semantic features. We further propose the randomized view and rectangular dropout data enhancement strategies to encourage the model to adapt to various scales of inputs and ignore frames with less geometric information, respectively. In addition, to further enhance the generalization of AnyView and consistent point cloud feature density, we propose a dynamic token strategy to adaptively adjust the number of extracted features per frame according to input frame count, which ensures the parameter compatibility and uniformity of the point cloud feature scale. AnyView fuses the multiview point cloud with camera parameters and refines the initial proposal with a transformer decoder based on the extracted scene representations. Extensive experiments on ScanNet show that our method outperforms previous methods in both accuracy and generalizability with a similar amount of parameters. In the online detection simulation on the ScanNet dataset, AnyView achieves 55.23% mAP@25, which is 14.14% higher than 3DETR [23].

II. RELATED WORK

Advances in 3D sensors have led to a surge of methods designed for 3D object detection with various modality. The large amount of related works can be divided into three groups based on the modality of 3D data. We also briefly discuss the sensors and datasets corresponding to these modalities.

Point-based 3D object detection: This kind of methods take in 3D scenes represented by pure point clouds, which are acquired by LIDAR sensor [10] or 3D reconstruction from

multi-view RGB-D images [5], [60], [9]. Early 3D object detection methods mainly include sliding-window methods [38] and template-based methods [17], [19]. Deep learning-based end-to-end 3D object detection methods began to emerge in recent years, which are mainly based on PointNet [31], [32] or sparse CNN [11] backbones. PointNet-based methods [35], [29], [23], [47] consume point clouds directly with the set abstraction operation [32], which enables flexible receptive fields for 3D feature learning. Sparse CNN-based methods [60], [42], [55], [8] project the point clouds to regular grids to be processed by advanced 2D or 3D CNN architectures. Tang *et al.* [41] further combine the two representations to learn more discriminative features. Liu *et al.* [20] proposed a dynamic point cloud joint detection framework, which uses spatio-temporal information to improve the problem of target loss due to severe occlusions.

Recently numerous works have employed bird’s eye view BEV to improve the point cloud feature extraction backbone network. Deng *et al.* [6] proposed the use of point cloud projection onto perspective views and BEV to capture multiview features, which employed a novel bilaterally guided multiview fusion block to phantom 3D representations leveraging the complementary information in perspective views and BEV. An *et al.* [1] designed a saliency detection task to enhance the detector for sparse point cloud object recognition, exploiting voxels and BEV saliency maps as asymptotic attention to resist redundant features in the background region. Xie *et al.* [51] proposed a novel local global feature adaptive aggregation mechanism to fuse contextual information at a fine-grained level and improve the quality of proposals with weighted relational awareness.

Several researchers have enhanced point cloud feature extraction by fusing information from multiple sources. Liu *et al.* [20] proposed a dynamic point cloud joint detection framework, which uses spatio-temporal information to improve the problem of target loss due to severe occlusions. Shan *et al.* [15] proposed to utilize the PTT module for modeling feature interactions between the voting phase and proposal generation phase of object detection, which enhances the feature extraction of sparse point cloud objects. However, point-based detection models have high inference latency due to inefficient sampling algorithms.

RGBD-based 3D object detection: RGBD camera is the mainstream 3D sensor for indoor scene understanding tasks. Existing RGBD-based 3D object detection methods take in monocular RGB-D image [24], [37] or point clouds reconstructed from multi-view RGB-D images (mentioned above). Here we only review the former methods which make full use of both RGB and depth information. Prior methods broadly fall into three categories: 2D-driven, 3D-driven, and modal fusion. 2D-driven methods [7], [52] first detect object in images and then use the results to assist search in 3D space. Pahwa *et al.* [25] proposed to utilize per-frame depth information and multi-view scene information to obtain accurate 3D object suggestions and generate 3D bounding boxes for potential 3D regions of interest. Kundu *et al.* [16] presented a microscopic rendering and comparison loss by employing voxel patterns to represent 3D objects, which allows 3D shapes and poses to be

learned via 2D supervision.

The most common approach to 3D-driven is to feed image information into a 3D feature extraction network as an additional channel to a point cloud or voxel. Song *et al.* [38] localized objects on a voxelized point cloud by sliding a 3D detection window, and category information was obtained from RGB pixels attached to the point cloud. Song *et al.* [39] proposed to process RGB-D inputs by sparse convolution and generate 3D proposals, and subsequently determine object categories by a designed joint object recognition network. However, this type of simple point cloud and image combination approach may destroy the fine-grained local geometric structural features of the point cloud, resulting in inefficient fusion between the point cloud and image modalities.

Modal fusion methods [22], [28] use the geometric correspondence between 2D and 3D to guide the predictions of the network and enrich the representation by concatenating multimodal features. Zhu *et al.* [62] employed virtual point cloud images to effectively bridge the resolution gap between image modality and point cloud modality to address the information loss due to multimodal data fusion. Bai *et al.* [2] employed Transformer to adaptively fuse 3D point cloud proposals with image features and processed difficult samples in the point cloud with an image-guided strategy, effectively improving the robustness of low-quality images. However, there is still a huge performance gap between RGBD-based methods and point cloud-based methods.

Multi-sensor 3D object detection: Recently, multi-sensor fusion has aroused increased interest in the 3D detection community. Depending on the fine-grained level of the fusion approach, existing approaches can be classified into region-level and point-level fusion methods.

Region-level fusion methods generate object proposals in 3D space and project them to images [4] or lift image proposals into a 3D frustum to reduce the search space in 3D space [30], [36]. Qi *et al.* [30] implemented multimodal inference directly employing a 2D object detector with a 3D point cloud feature extraction network, this framework was able to maintain high accuracy even in the presence of strong occlusions or very sparse points and inspired a series of subsequent work Wang *et al.* [48] proposed to project region proposals on 2D images as frustums in 3D space and utilize 3D backbone network extraction to achieve region-level feature fusion. Liu *et al.* [21] proposed a fusion module based on a depth-attention mechanism to achieve multimodal feature differential fusion at various depths and addressed the unstable efficiency of modal fusion of point clouds and images. Paigwar *et al.* [26] extended the fusion approach to pillar representation and proposed a novel masked point cloud approach to improve object localization accuracy.

Point-level fusion methods, on the other hand, usually enhance the LIDAR points with the image semantic features. There are several researches aiming to enhance the input point cloud with image features and then employ a 3D object detector to process the enhanced point cloud for higher accuracy. The image features can be fused to input LIDAR points [44], [56] or middle feature points [59], [50]. Xu *et al.* [53] utilized point-to-pixel projection matrices to attach 2D

semantic segmentation labels to 3D point clouds and employed an attentional mechanism to adaptively fuse semantic information to significantly improve model performance. Yin *et al.* [56] proposed to generate a dense 3D virtual point cloud via a 2D images object detector to solve the point cloud sparsity problem and this approach can be naturally integrated into any LiDAR data. Vora *et al.* [44] proposed to project 3D point cloud information to the 2D image semantic segmentation results and can feed the integrated information back to any 3D point cloud object detection models, which provides a better trade-off between accuracy and speed. After that, point-based methods are adopted to detect objects from the decorated point clouds. However, effectively fusing information from multiple modalities remains an open challenge.

III. ANALYSIS

In this section, we first describe the problem statement from existing benchmarks for indoor 3D object detection. Then we propose a more unified and reasonable setting for indoor 3D object detection task. Finally we show the failing case of previous models in practical scenarios.

A. Problem Statement

In order to better utilize 3D detector in practical tasks where the raw input is a variable number of RGB-D images, we propose a new setting for indoor 3D object detection.

Inference: Unlike the input data format of the existing benchmarks, in order to simulate the inference process of the model in the practical scene, we take the sparse RGB-D images and their camera parameters as the unified input data of the 3D detector to provide the intelligent body with the scene object detection results, which can be summarized as follows:

$$\mathcal{B}_N = \mathcal{D}(\{I_k, R_k^c, T_k^c\}_{k=1}^N), R_k^c \in \mathbb{R}^{3 \times 3}, T_k^c \in \mathbb{R}^{3 \times 1} \quad (1)$$

where N represents the number of RGB-D image frames input to the 3D object detector \mathcal{D} , and \mathcal{B}_N represents the reconstructed point cloud detection results of N frames of RGB-D images. I_k , R_k^c , and T_k^c correspond to the k_{th} frame of RGB-D image, rotation matrix, and translation matrix, respectively. $\{I_k, R_k^c, T_k^c\}_{k=1}^N$ can represent both local region and a whole scene. To reduce the time for data collection, the maximum number of views is set to 50 ($N \leq 50$), which is far less than the number required for 3D reconstruction.

Model: Since the number of input views will change according to the task in practical scene deployments, the 3D object detectors \mathcal{D} must be highly flexible in order to efficiently process RGB-D images with the variable number of frames input. Therefore, the training process of models \mathcal{D} needs to incorporate adaptations which enable \mathcal{D} to process point clouds with arbitrary scale inputs without additional fine-tuning. This attribute significantly improves the utility and efficiency of the 3D detection applications, enabling them to easily handle a wide range of task input scenes and provide accurate object detection results.

Evaluation: The performance of model should not be evaluated only on one scale of input. We prepare a variety of validation sets containing different scales of input

TABLE I
GENERALIZABILITY OF PREVIOUS MODEL. THE GRAY CELL INDICATES
ON WHICH BENCHMARK THE MODEL IS TRAINED.

	ScanNet-SV	ScanNet-Rec	ScanNet-MV
ImVoteNet	31.6 / 13.5	–	43.3 / 20.4
3DETR	19.8 / 6.1	64.5 / 44.0	44.7 / 25.6

data, such as monocular input, few-view input and scene-level input. The number of views N can range from 1 to 50. Two representative methods are chosen: ImVoteNet [28] for monocular RGB-D input and 3DETR [23] for scene-level point cloud input. We prepare three benchmarks from the raw RGB-D videos provided by ScanNet: ScanNet-SV, ScanNet-Rec, and ScanNet-MV¹. ScanNet-SV (single view) is a monocular RGB-D benchmark organized similar to SUN-RGBD. ScanNet-Rec (reconstruction) is the previous scene-level benchmark. ScanNet-MV (multi-view) shares the same ground truth with ScanNet-Rec but provides multi-view RGB-D images as input instead of reconstructed point clouds.

We train ImVoteNet and 3DETR on ScanNet-SV and ScanNet-Rec respectively and evaluate the models on all benchmarks. When applying 3DETR on ScanNet-MV, we fuse the multi-view depth maps into point clouds according to the camera parameters. As for applying ImVoteNet on ScanNet-MV, we predict bounding boxes for each view and fuse the results by 3D NMS. As shown in Table I, 3DETR trained on reconstructed point clouds performs poorly on the monocular RGB-D benchmark, and both ImVoteNet and 3DETR fail to achieve a satisfactory performance on the multi-view RGB-D benchmark. This experimental result indicates that the performance of the detector on previous benchmarks may not reflect its performance in practical applications. And the poor generalizability of previous models poses a huge challenge in applying the existing models in practical tasks, where time for data collection is limited and the scale of input data is changeable.

IV. APPROACH

In this section, we propose a new framework called AnyView for detecting 3D objects from multi-view RGB-D images. We first show the overall framework of AnyView. Then we introduce the input scale-independent training strategy. Finally we detail the dynamic token technique for accuracy-computation tradeoff during inference time.

A. Overall Framework

The overall framework of AnyView is illustrated in Fig. 2. Given multi-view RGB-D images as input, AnyView focuses on the utilization of depth maps and camera parameters. We will introduce our method in detail as follows.

Formally, the images are represented by $\{I_1, I_2, \dots, I_N\}$. We sample K points for each depth map and convert them into camera coordinate by intrinsic camera calibration matrix, which are denoted as $\{P_{c1}, P_{c2}, \dots, P_{cN}\}$, $P_{ci} \in \mathbb{R}^{K \times 3}$. The rotations and translations from camera coordinate to world coordinate for each view are $\{R_1^c, R_2^c, \dots, R_N^c\}$ and $\{T_1^c, T_2^c, \dots, T_N^c\}$.

¹Refer to Section V-A for more details.

Extract scene proxies: Previous 3D detection methods are only able to process point clouds as a whole. So a natural solution for consuming multi-view RGB-D images is to fuse the depth maps into a whole scene $P = \mathcal{C}(R_i^c \cdot P_{ci} + T_i^c)$, where \mathcal{C} denotes concatenation operation. However, point clouds generated from different numbers of views vary a lot in local geometry structure and global semantics, which will lead to deteriorated scene representation when numbers of view for training and inference are not the same. To decouple scene representation with the scale of input data, we propose to extract T scene proxies for each view independently with a shared geometry learner:

$$\mathcal{P}_i = G(P_{ci}), \mathcal{P}_i \in \mathbb{R}^{T \times C} \quad (2)$$

Scene proxies \mathcal{P}_i are local feature descriptors which represent the geometry structures of single view point clouds. We implement the geometry learner G as two set abstraction (SA) layers [32], the first layer with a constrained receptive field to focus on local geometric details and the second with a large receptive field to aggregate the local details into geometry structures. As G is applied on each view independently, the extracted scene proxies will ignore global semantics and be robust to the scales of input data.

Interactions among scene proxies: We obtain richer scene representations through interactions among scene proxies. In order to keep the input scale-independent property of scene proxies, we hope the interaction to be linear combination $\mathcal{P}_{ij} = \sum_{i=1}^N \sum_{j=1}^T \alpha_{ij} \mathcal{P}_{ij}$, where $\sum_i \sum_j \alpha_{ij} = 1$. In addition, since the number of view (N) is variable, the number of interacting scene proxies is also variable. Benefiting from the nature of self-attention, these requirements can be elegantly achieved by transformer [43].

Specifically, we first mix the scene proxies in world coordinates by transforming their coordinates:

$$\{\mathbf{P}_{ij}^x, \mathbf{P}_{ij}^y, \mathbf{P}_{ij}^z\} = R_i \cdot \{\mathbf{P}_{ij}^x, \mathbf{P}_{ij}^y, \mathbf{P}_{ij}^z\} + T_i \quad (3)$$

where $\mathbf{P}_{ij}^{x,y,z}$ represents the spatial position of \mathcal{P}_{ij} in the camera coordinate system, and we project them into the world coordinate system to obtain global information at a higher level with the camera projection matrix. Then the scene proxies are fed into the transformer encoder with their coordinates converted into Fourier positional embeddings [40]. We adopt radius mask [23] on the self-attention matrix to conduct interactions from local to global.

Decode objects from the whole scene: Given the $N_T = N \times T$ features from the encoder, we adopt a transformer decoder to refine object queries layer by layer as in DETR [3]. The object queries are initial proposals, which are generated by furthest point sampling from the whole scene to ensure coverage:

$$\mathbf{Q} = \mathcal{M}(\mathcal{F}(\mathcal{C}(R_i^c \cdot P_{ci} + T_i^c))) \quad (4)$$

where \mathcal{M} represents the MLP and \mathcal{F} represents the furthest point sampling algorithm. The refined queries are converted into box parameters and supervised following the procedure in 3DETR [23].

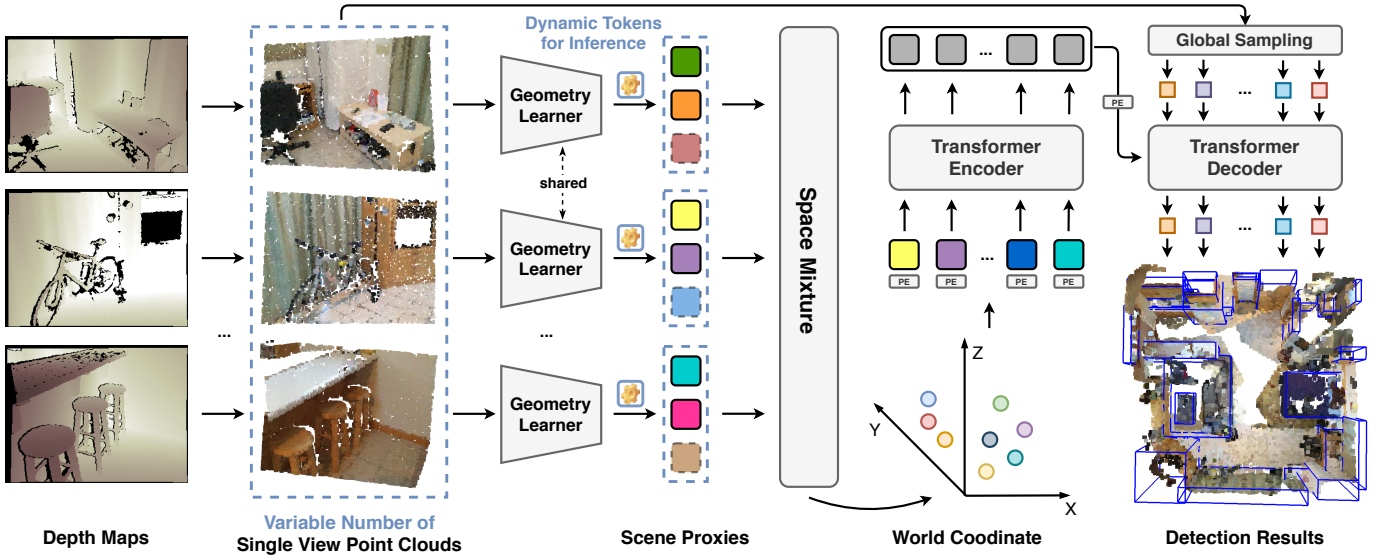


Fig. 2. The framework of AnyView. Given multi-view RGB-D images of variable number, we first convert the depth maps to single view point clouds according to intrinsic camera parameters. Then a shared geometry learner is applied to extract scene proxies for each view, which are local feature descriptors independent of input scale. Scene proxies from different views are mixed into world coordinates according to the extrinsic camera parameters. We adopt transformer encoder to refine the scene proxies while keeping their input scale-independent property by self-attention mechanism. A transformer decoder is used to refine the object proposals, where the initial proposals are sampled from the whole scene by FPS. The dashed blue box indicates the number of inside elements is changable during inference.

B. Scale-independent Training

Although the architecture design of AnyView can extract features independent of input scale and detect 3D objects from any number of views, we find proper data augmentation is essential for training the model, which are listed below.

Random view dropping: During training, the numbers of views of different inputs in a batch are kept the same in order to parallelize the computation. However, enabling the network to process variable number of views is necessary as it encourages the transformer to adapt to different scale of attention map. To this end, we randomly drop 0 to $\frac{N}{2}$ views and pad the dropped points with 0. To cut down the interactions between the dropped scene proxies and other tokens (scene proxies for encoder, object queries for decoder), we apply a binary mask on each attention map to indicate which of scene proxies are invalid (with coordinates $(0, 0, 0)$). The binary mask will set the inner products between invalid scene proxies and other tokens to $-\infty$, so after softmax operation these attention value will be 0.

Global random cuboid: The geometry structure of single view point clouds may vary from view to view. For example, when the distance between the RGB-D camera and the scene varies, the density of point clouds varies as well. When one view only contains floors and walls, the scene proxies extracted from it are uninformative. To allow the network to handle depth maps taken from various shooting situations and learn to ignore scene proxies with less information, we randomly crop a cuboid [58] from the fused point clouds $P = \mathcal{C}(R_i^c \cdot P_{ci} + T_i^c)$ and set other points outside the cuboid to $(0, 0, 0)$. After that, we transform the point clouds back to the camera coordinates of each view and keep $(0, 0, 0)$ unchanged. This strategy mak some views lose geometric information but still provide valid scene proxies, which effectively reduces overfitting and improves the generalizability of AnyView.

C. Dynamic Tokens for Inference

AnyView extracts N_T scene proxies for a N -view input scene. In our setting, N may vary from 1 to 50 during inference time, which results in an order of magnitude change in the number of scene proxies. In previous work such as VoteNet [29] and 3DETR [23], the encoder of detector extract 1024 or 2048 seed points for one scene, no matter monocular RGB-D input or scene-level point clouds input. To reach this order of magnitude, T should be around 40 when $N = 50$ and be around 2000 when $N = 1$. For the former case, AnyView only extracts 40 scene proxies for monocular input, which is not enough to fully represent the scene. While for the latter case, the number of scene proxies will be larger than 10000 when there are more than 10 views. This heavy computation cost is unaffordable in practical applications.

To our best knowledge, all previous networks which use SA layers to extract point features keep a fixed output point number during training and inference. However, as the parameters in SA layer are only relevant with the number of channels, changing the output number seems feasible. The reason why previous methods fix the output number are two-fold: 1) if the output number of a SA layer is changed, the shape of input tensor for the next layer will change and may be incompatible with the parameters; 2) even if the next layer can process input in dynamic shape, the density of point clouds in this level is different from the one during training, which makes the layer unable to extract accurate feature representation. To overcome this problem in our case, we devise a dynamic token strategy for the geometry learner by keeping the output number of the first SA layer fixed and change the output number of the second one. Thus T can be defined as:

$$T = \min\{Z/N, O_{SA_1}\} \quad (5)$$

where Z is a predefined constant and O_{SA_1} is the the output

TABLE II
NUMBER OF PARAMETERS OF DIFFERENT 3D DETECTORS.

ImVoteNet	ImVoxelNet	3DETR-m	AnyView
1.8M	104.6M	7.4M	7.6M

number of the first SA layer. In this way, the second SA layer receives the same number of input points as in training time and thus the output features (i.e. scene proxies) are accurate. Although the number of scene proxies varies, the transformer encoder is still able to interact and refine them due to the linear combination nature of self-attention mechanism and our scale-independent training strategy.

Meanwhile, our proposed AnyView can be well applied to the online detection task as it extracts features \mathcal{P}_i individually for each view V_i when processing RGB-D inputs and then integrates the features of different views $\{\mathcal{P}_1, \dots, \mathcal{P}_i\}$ in the world coordinate system through an attention mechanism. The ability to detect objects online fast and accurately in dynamic 3D scenes is crucial for autonomous navigation, environment understanding, and other tasks in the field of autonomous driving and robotics. Our proposed method provides a reliable and efficient solution for online detection, which can enable robots to effectively perceive and interact with the environment.

V. EXPERIMENT

In this section, we conduct experiments to show the generalizability of our approach. We first describe the datasets and experimental settings. Then we comprehensively compare our approach with previous indoor 3D object detection methods on a series of benchmarks. Visualization results are provided for more intuitive comparison. Finally we design several ablation studies to verify the effectiveness of our architecture design and training/inference strategies.

A. Experiments Setup

Datasets and benchmarks: We conduct experiments on the ScanNet [5] dataset, which is a richly annotated dataset of indoor scenes with 1201 training scenes and 312 validation scenes. For each scene, ScanNet provides RGB-D video as well as the reconstructed mesh. We uniformly sample 50 frames from the video for each scene, which serves as the maximum data available for training and evaluating in our proposed setting. Meanwhile, we further validate that the proposed approach has the ability to accurately detect objects in practical deployment scenes by verifying the performance of each model on the online detection task. We set three benchmarks as defined in Section III-A. ScanNet-Rec is the mainstream scene-level benchmark used by previous works [14], [29], [23], whose input data is reconstructed point cloud of a whole scene and ground-truth is generated by computing the axis-aligned bounding boxes [14] for objects in 18 selected categories. In addition, we designed ScanNet-Online benchmarks to explore the performance of previous 3D object detection models with AnyView in practical deployment scenes. Specifically, the input to ScanNet-Online is each frame in a sequence of RGB-D images, and the model needs to dynamically detect objects in the scene based on the new input frames. ScanNet-MV shares the same ground truth with

TABLE III
3D OBJECT DETECTION RESULTS (MAP@0.25 AND MAP@0.5) AND CORRESPONDING TRAINING/INFERENCE SETTING OF DIFFERENT METHODS ON SCENE-LEVEL AND MONOCULAR BENCHMARKS. CONTENTS IN BRACKET INDICATE THE MODALITY USED BY THE METHODS.

	Method	Training Benchmark	Evaluation Benchmark	mAP	
				@0.25	@0.5
Scene-level	3DETR	Rec	Rec	62.7	37.5
	3DETR-m	Rec	Rec	65.0	47.0
	3DETR	MV(D)	Rec	53.6	33.0
	3DETR-m	MV(D)	Rec	56.9	37.8
	3DETR	Rec	MV(D)	37.8	22.2
	3DETR-m	Rec	MV(D)	44.7	25.6
	VoteNet	SV(D)	MV(D)	40.9	20.6
	ImVoteNet	SV(RGBD)	MV(RGBD)	43.3	20.4
	ImVoxelNet	MV(RGB)	MV(RGB)	46.6	25.2
	3DETR	MV(D)	MV(D)	51.7	31.0
	3DETR-m	MV(D)	MV(D)	54.7	35.3
	AnyView	MV(D)	MV(D)	60.7	35.8
Monocular	VoteNet	SV(D)	SV(D)	30.1	13.9
	ImVoteNet	SV(RGBD)	SV(RGBD)	31.6	13.5
	3DETR	Rec	SV(D)	14.7	3.9
	3DETR-m	Rec	SV(D)	19.8	6.1
	ImVoxelNet	MV(RGB)	SV(RGB)	21.2	8.3
	3DETR	MV(D)	SV(D)	24.7	10.9
	3DETR-m	MV(D)	SV(D)	27.7	12.8
	AnyView	MV(D)	SV(D)	32.7	15.3

ScanNet-Rec, while the input data are multi-view RGB-D images. If not additionally mentioned, the default number of views is 50. ScanNet-MV is also a scene-level benchmark, which means all RGB-D images from one scene are considered as a single input sample for the network. ScanNet-SV is a monocular RGB-D benchmark with a single view RGB-D image as input data. For each image, we select the bounding boxes whose center points are within the image from the corresponding scene as its ground truth.. ScanNet-Online utilizes the ScanNet-MV benchmark in the 50 views setting, and the input is each frame of sequential RGB-D images.

Compared methods: We train VoteNet [29] and ImVoteNet [28] on ScanNet-SV. When applying the models on ScanNet-MV, we predict bounding boxes for each view and fuse the predictions by 3D NMS. 3DETR [23] is chosen as the model trained on ScanNet-Rec, which is the mainstream transformer-based 3D detector with less inductive bias. The comparison between 3DETR and AnyView is particularly relevant since they share similar amount of parameters and both adopt DETR-like detection decoder. To apply 3DETR on ScanNet-MV, we preprocess the multi-view RGB-D images by fusing the depth maps from each view according to the camera parameters. We train our AnyView model as well as 3DETR and ImVoxelNet [34] on ScanNet-MV, each model representing an input modality: 3DETR for scene-level point clouds, ImVoxelNet for multi-view RGB and AnyView for multi-view RGB-D. We list the number of parameters of these models in Table II.

Implementation details: We downsample the RGB-D videos from ScanNet to a resolution of 320×240 . Following

TABLE IV

3D OBJECT DETECTION RESULTS (MAP@0.25 AND MAP@0.5) OF DIFFERENT MODELS ON SCANNET-SV AND SCANNET-MV. HERE SCANNET-MV IS FURTHER DIVIDED ACCORDING TO THE NUMBER OF VIEWS AND HOW THESE VIEWS ARE COMBINED. UNIFORM/CONTINUOUS MEANS THE VIEWS ARE SAMPLED UNIFORMLY/ADJACENTLY FROM THE WHOLE 50 VIEWS. GRAY CELLS SHOW ON WHICH BENCHMARK THE MODEL IS TRAINED.

	Methods	ScanNet-SV	ScanNet-MV					
			5	10	15	30	40	50
Uniform	ImVoteNet	31.6 / 13.5	30.2 / 13.7	37.3 / 17.9	40.3 / 18.5	43.5 / 20.6	42.9 / 20.4	43.3 / 20.4
	3DETR-m(10)	29.8 / 12.5	39.7 / 20.0	49.1 / 28.0	50.8 / 29.0	50.3 / 28.9	49.6 / 28.9	48.9 / 27.7
	3DETR-m(30)	29.1 / 13.1	36.8 / 19.5	50.1 / 29.6	53.1 / 31.4	55.6 / 33.9	55.7 / 34.3	55.6 / 34.7
	3DETR-m(50)	27.7 / 12.8	34.9 / 17.9	48.6 / 29.0	52.5 / 33.3	55.3 / 36.3	55.6 / 35.9	54.7 / 35.3
	AnyView(10)	31.3 / 13.7	42.2 / 20.4	51.3 / 27.2	52.8 / 29.0	53.2 / 29.9	54.9 / 30.4	54.8 / 30.1
	AnyView(30)	30.5 / 12.7	39.8 / 20.1	52.4 / 29.2	57.1 / 31.6	59.1 / 35.2	59.9 / 36.8	60.1 / 37.4
	AnyView(50)	32.7 / 15.3	45.0 / 22.0	53.8 / 30.5	57.5 / 33.5	59.5 / 35.7	60.6 / 35.7	60.7 / 35.8
Continuous	ImVoteNet	31.6 / 13.5	18.1 / 8.8	25.2 / 13.5	30.4 / 15.7	40.5 / 18.4	43.1 / 20.0	43.3 / 20.4
	3DETR-m(10)	29.8 / 12.5	19.9 / 9.9	27.7 / 15.3	34.0 / 18.1	44.2 / 24.1	48.7 / 27.8	48.9 / 27.7
	3DETR-m(30)	29.1 / 13.1	18.5 / 9.6	26.6 / 15.1	35.4 / 19.7	48.0 / 29.4	54.0 / 33.6	55.6 / 34.7
	3DETR-m(50)	27.7 / 12.8	17.9 / 9.7	26.6 / 15.8	34.9 / 19.8	46.9 / 28.8	52.7 / 33.0	54.7 / 35.3
	AnyView(10)	31.3 / 13.7	20.6 / 10.6	30.2 / 15.7	36.0 / 17.7	47.9 / 26.1	53.6 / 28.7	54.8 / 30.1
	AnyView(30)	30.5 / 12.7	19.9 / 10.1	29.9 / 16.5	36.8 / 21.4	52.3 / 30.0	57.1 / 34.3	60.1 / 37.4
	AnyView(50)	32.7 / 15.3	22.1 / 11.3	32.9 / 18.6	40.6 / 21.8	54.4 / 29.8	58.7 / 34.4	60.7 / 35.8

previous setting [29], we sample 20000 points per scene for ScanNet-SV and 40000 points per scene for ScanNet-Rec as the input point clouds. For ScanNet-MV, we sample 20000 points per view for methods that make predictions on each view independently and sample 40000 points per scene for methods that fuse multi-view point clouds as a whole. While for AnyView, we sample 5000 points per view to reduce computation cost.

The geometry learner of AnyView consists of two SA layers, the first with radius $0.2m$, output number of points 256 and MLP channels [3, 64, 128, 256], the second with radius $0.8m$ and MLP channels [256, 256, 256, 256]. During training, we set $T = 40$. While in inference time, we set $Z = 2000$. Following the configurations of 3DETR-m, we adopt 3 transformer encoders and 8 decoders in AnyView. The radius mask for encoder is set to $[0.8m, 0.8m, 1.2m]$. In terms of data augmentation, both random view dropping and global random cuboid are applied with probability 0.75.

As for the online detection setting, in processing the online detection RGB-D input flow $F = \{f_1, \dots, f_i\}$, our proposed AnyView will save the extracted \mathcal{P}_i for each RGB-D image frame f_i , at the input of the next RGB-D frame f_{i+1} , it will directly read $\{\mathcal{P}_1, \dots, \mathcal{P}_i\}$, which will be fed into the detector along with \mathcal{P}_{i+1} to predict the result.

B. Results and Analysis

On scene-level and monocular benchmarks: We show the performance of different models on scene-level (Rec and MV) and monocular (SV) benchmarks in Table III. As discussed in Section III-A, previous models trained on ScanNet-Rec or ScanNet-SV generalizes poorly to other settings. Although 3DETR-m trained on ScanNet-Rec achieves the best performance (65.0/47.0) on scene-level benchmarks when evaluated on ScanNet-Rec, it requires reconstructed point clouds which are not available in many practical scenarios. We find 3DETR-m trained on ScanNet-MV gets lower performance (54.7/35.3) on scene-level benchmarks, which indicates the previous ScanNet-Rec benchmark is too idealistic and the

point clouds fused from multi-view depth maps are more challenging for 3D object detection. Among models trained on ScanNet-MV, ImVoxelNet gets relatively lower performance as color is less informative than depth, especially for 3D object detection. 3DETR-m generalizes better to single view inputs (54.7/35.3) when trained on ScanNet-MV, which shows ScanNet-MV is not only a more practical benchmark for evaluation, but also beneficial for training a generalizable 3D detector. Observing the rows in gray, AnyView achieves leading result (60.7/35.8) on the challenging ScanNet-MV benchmark and also generalizes well (32.7/15.3) to ScanNet-SV, which even outperforms ImVoteNet (31.6/13.5) trained on ScanNet-SV.

On wider range of input views: We further extend ScanNet-MV to a series of fine-grained benchmarks for more comprehensive analysis. We train models on 10/30/50 views uniformly sampled from the whole 50 views in ScanNet-MV and evaluate them on different numbers of views. We devise two settings for partial scenes: Uniform and Continuous, indicating the evaluation of model is conducted on uniformly/adjacently sampled views. As shown in Table IV, 3DETR-m trained on small number of views gets low performance on large number of views, and vice versa. On the contrary, with the growing of numbers of training views, AnyView shows consistent improvement across various scales of input. Even if combining the best results of three 3DETR-m models, AnyView still surpasses them by a large margin with a single set of parameters.

The detection results of 3DETR-m and AnyView after NMS is shown in Fig. 3, where a whole scene consisting of 50 views and a part of it consisting 10 adjacent views are chosen as the input. 3DETR-m fails to detect any of the doors for the whole scene. That is because 3DETR-m fuses multi-view point clouds as a whole, which makes the detector hard to focus on thin objects like doors and windows whose geometric information is weak. It also aggregates outliers into misleading clusters, resulting in false positive. On the contrary, AnyView extracts scene proxies for each view independently, which owns better understanding of local geometry structures and

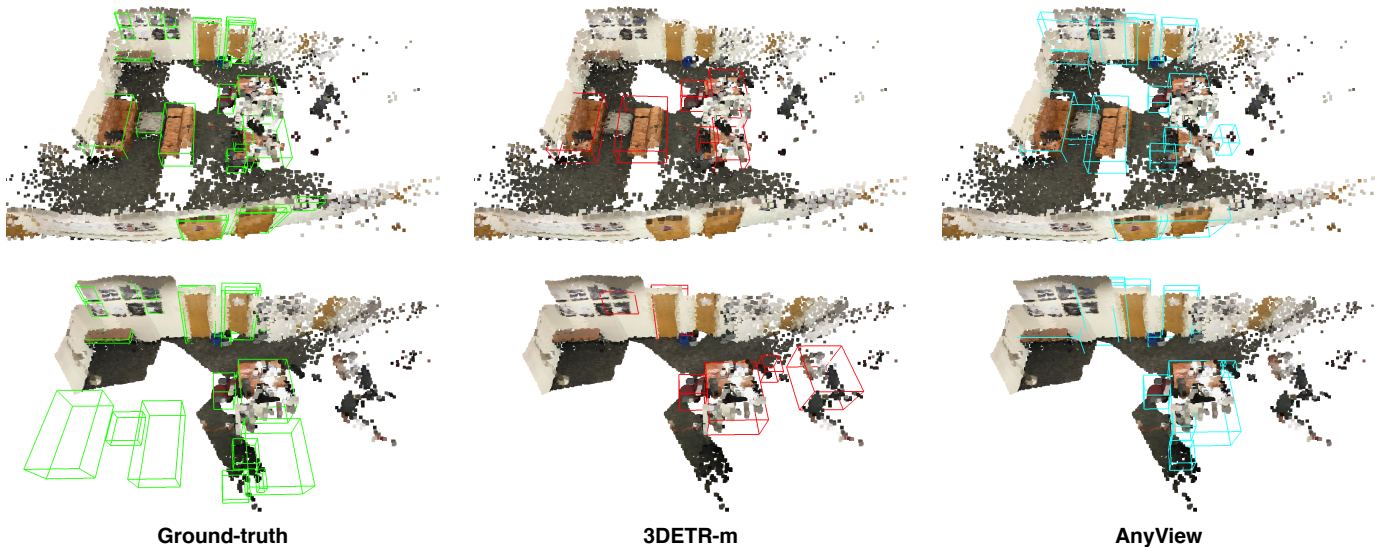


Fig. 3. Visual results on ScanNet. We compare the predictions of 3DETR-m and AnyView after NMS with the ground-truth bounding boxes on different scales of input. Top: the whole scene consisting of 50 views, Bottom: a part of scene consisting of 10 adjacent views. AnyView successfully detects all the doors without color information, which shows its strong ability for extracting local geometric information. The predictions of AnyView is also more consistent across different input scales.

successfully detects all the doors for both scenes. Benefiting from the input scale-independent property, AnyView outputs consistent predictions for different input scales.

C. Ablation Study

We conduct ablation studies to show how different architecture designs and training/inference strategies influence the performance of the proposed AnyView framework. The models are trained on ScanNet-MV with 30 views.

Performance w.r.t. architecture design: We ablate three parts of architecture designs of AnyView, as shown in Table V. GlobalQuery indicates the object queries are sampled from the concatenated scene (\checkmark) instead of the coordinates of scene proxies. CoordsTrans means whether to apply geometry learner in the camera coordinate (\checkmark) of each view or in the world coordinate. PE_{enc} indicates whether to use positional embeddings for the transformer encoder. The first two rows show that high object query coverage of the scene is beneficial for the transformer decoder. The third row shows unifying the coordinate makes the geometry learner extract more robust scene proxies. As the features of point clouds already contain positional information, 3DETR finds positional embeddings are not necessary. However, in AnyView the scene proxies are independently extracted, so the spatial relationship between scene proxies from different views is weakened. We find Fourier positional embeddings with a MLP performs best.

Performance w.r.t. data augmentations: We further investigate the effects of two proposed data augment strategies. ScanNet-MV measures the detection accuracy and ScanNet-SV measures the generalizability of the detector. As shown in Fig. 4, with the growing of minimum keeping ratio for random view dropping, the performance of AnyView on ScanNet-MV grows but its generalizability to single view input has deteriorated. In terms of the probability of augmentation, it is shown that low probability leads to overfitting and poor generalizability, while very high probability hurts the performance

TABLE V
THE EFFECTS OF GLOBAL QUERY SAMPLING, COORDINATE TRANSFORMATION AND POSITIONAL EMBEDDINGS FOR TRANSFORMER ENCODER ON THE FINAL PERFORMANCE OF ANYVIEW ON SCANNET-MV.

GlobalQuery	CoordsTrans	PE_{enc}	mAP	
			@0.25	@0.5
\checkmark			58.5	33.1
\checkmark			59.2	34.4
\checkmark	\checkmark	Fourier	59.6	34.9
\checkmark	\checkmark	MLP \circ Fourier	60.1	37.4

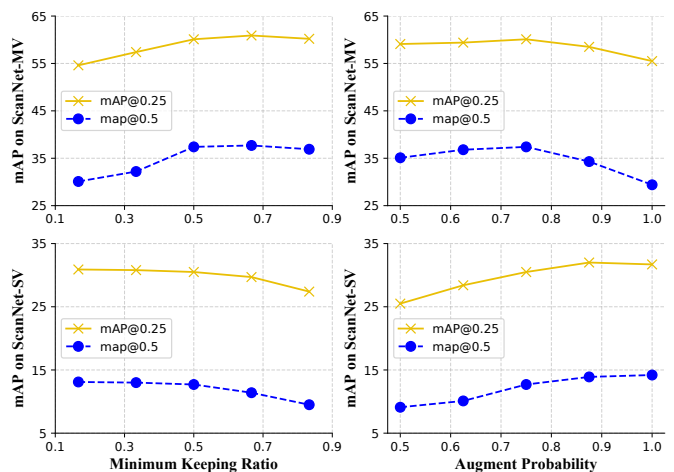


Fig. 4. The effects of minimum keeping ratio for random view dropping and probability for data augmentation on the final performance of AnyView on ScanNet-MV and ScanNet-SV.

of AnyView. Therefore we choose dropping $[0, \frac{N}{2}]$ views and augmenting with probability 0.75.

Performance w.r.t. number of tokens: Fig. 6 illustrates the effects of our dynamic token strategy, where the number of scene proxies for each view is $T = \min\{X/N, 256\}$, $X \in \{500, 1000, 2000, 4000\}$. We find when the number of scene proxies is too small ($N_T \leq 1000$), the performance of

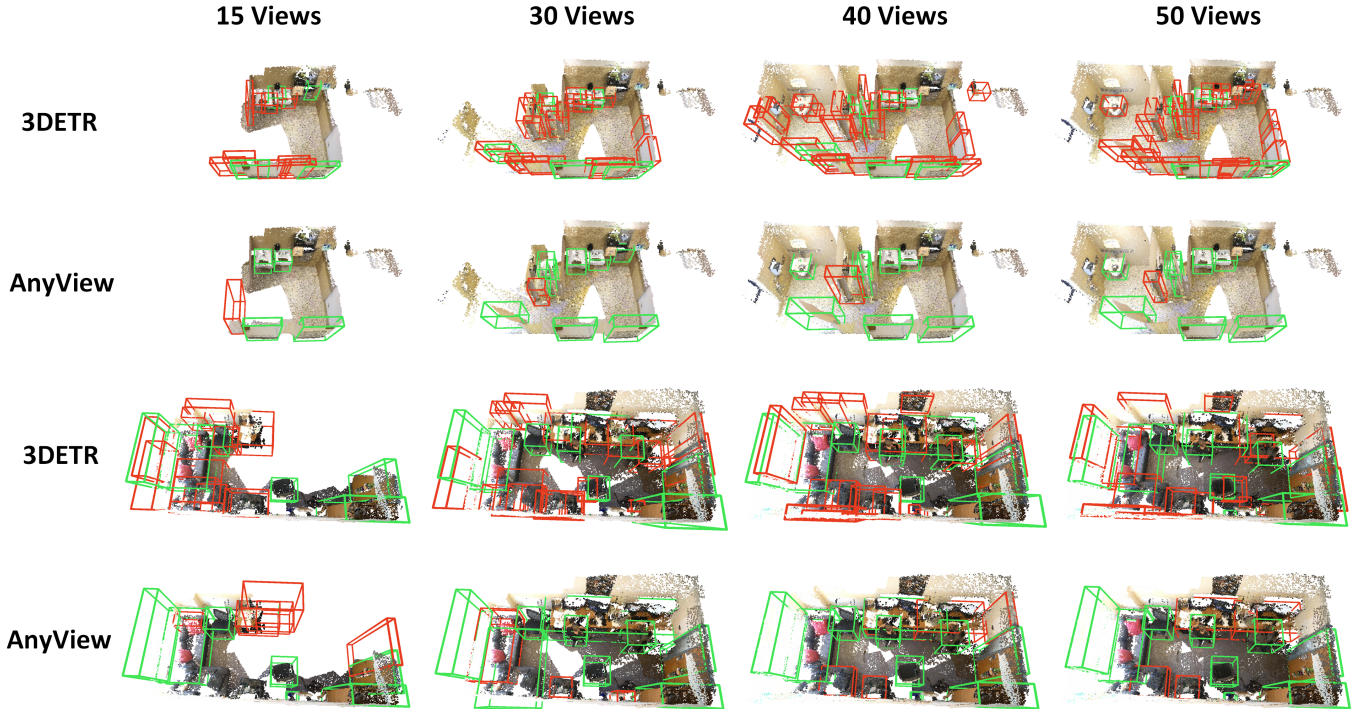


Fig. 5. Online detection visualization results. We demonstrate the detection results for 15, 30, 40, and 50 frames during the navigation(scene0086_00, scene00430_00 and scene0474_00 on the ScanNet dataset). Red bounding boxes and green bounding boxes represent false-positive and true-positive samples, respectively.

AnyView will even drop with the growth of view numbers. With the increasing number of N_T , the performance of AnyView is significantly improved for any view number. However, when N_T is greater than 2000, the rate of performance increase decreases significantly, introducing additional computational cost without sufficient performance improvement, and $N_T = 4000$ even leads to a decrease in accuracy. So finally we set $N_T = 2000$ for a better trade-off between performance and cost.

D. Online 3D Object Detection

We conduct online object detection experiments to demonstrate the performance of AnyView with any-scale point cloud input. We select 3DETR as the baseline network, and these models are all trained on ScanNet-MV with 50 views. During the validation process, the views of each scene are fed into AnyView in a frame-by-frame format, and the aggregated point cloud reconstruction results are fed into the 3DETR.

Quantitative results: We demonstrate the average accuracy of AnyView and 3DETR in the online detection setting, as illustrated in Table VI. Our proposed AnyView achieves an average accuracy of (55.32/30.94) in the online detection setting. Compared to the MV(D) setting, which only decreases by 5.47 and 4.86 on the mAP@25 and mAP@50 measures, respectively. However, since 3DETR is unable to adapt to any size point cloud, the accuracy decreases significantly in the online setting, by 13.61 vs. 11.48, respectively. Meanwhile, we have visualized the curve of model performance with frame rate, as shown in Fig. 7. As the number of input RGB-D frames is too few, both AnyView and 3DETR are less accurate due to the sparse point cloud, though AnyView still outperforms

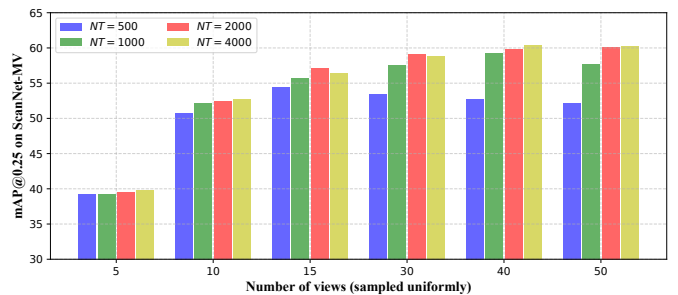


Fig. 6. The effects of token number during inference on the final performance of AnyView on ScanNet-MV.

3DETR by 7.26 vs. 6.68. As the number of input RGB-D frames increases, AnyView improves accuracy at a faster rate and stabilizes (View Number = 10). Meanwhile, the accuracy of AnyView has reached 52.78 vs. 29.18, which is only 6.71 vs. 6.64 lower than the overall scene. However, the accuracy of 3DETR has been improving with the number of reconstructed scene frames due to the failure to adapt to sparsely distributed scene point clouds. The performance of 3DETR stabilizes only after 40 frames of RGB-D image reconstruction and is 4.62 lower on the mAP@25 measure compared to AnyView. All the above results indicate that our proposed AnyView can be able to handle scene point clouds of any size and has the ability of online detection.

Qualitative results: We visualize the detection results of AnyView with 3DETR at different frame numbers as illustrated in Fig. 5. In the case of a large degree of site cloud fragmentation (15 Views), 3DETR has more false-positive samples, while AnyView still maintains a high detection accuracy. As the number of viewpoints of the reconstructed scene point cloud increases, the false-positive samples detected

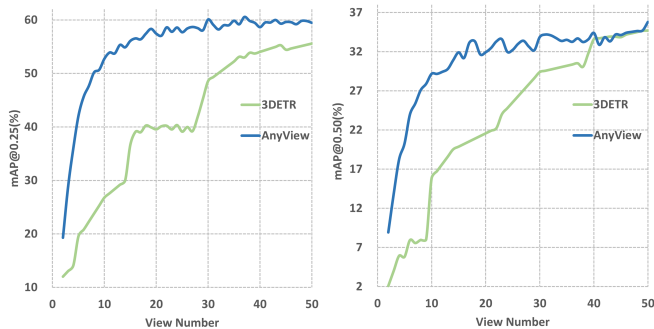


Fig. 7. The effect of the number of image frames on the overall scene detection accuracy in the Online setting.

TABLE VI

3D OBJECT DETECTION RESULTS AT THE ONLINE SETTING (MAP@0.25 AND MAP@0.5), WHERE S-L DENOTES SCENE-LEVEL

	Method	Training Benchmark	Evaluation Benchmark	mAP	
				@0.25	@0.5
S-L	3DETR	MV(D)	Online	41.09	23.82
	AnyView	MV(D)	Online	55.23	30.94

by 3DETR are suppressed to some extent, and better results are achieved at 50 Views. While the detection results of AnyView remain stable, the increase in the number of viewpoints does not lead to a significant increase in performance. The best performance is also achieved at 50 Views. The visualization results of online detection further demonstrate that the proposed AnyView can efficiently handle input scenes with different numbers of views and has the capability of online detection.

VI. CONCLUSION

In this paper, we challenge the existing benchmarks for indoor 3D object detection in a perspective of input data. We propose a new practical setting for this task, which unifies the input modality as multi-view RGB-D images with variable input frame numbers and evaluates 3D detectors on various scales of input data. We design a new transformer-based framework named AnyView for practical applications, which is able to process scenes consisting of any number of frames and extract input scale-independent scene representations. Benefiting from the nature of the self-attention mechanism and our scale-independent training strategy, AnyView is able to change the number of scene representations extracted for each input frame during inference and flexibly handle various numbers of input frames. Extensive experiments on the ScanNet dataset show that AnyView achieves both great generalizability and high detection accuracy while containing a similar amount of parameters with the baselines.

The main limitation of this work is the weak generalization to new categories of objects in practical scenes. Meanwhile, the dynamic token mechanism is only adaptive in terms of quantity, which may lead to loss of information. Future work hopes to achieve dynamic adaptation with token pruning techniques and open vocabulary detection.

ACKNOWLEDGEMENTS

This work was supported in part by the National Natural Science Foundation of China under Grant 62376032, Grant U22B2050, and Grant 62125603.

REFERENCES

- Pei An, Yucong Duan, Yuliang Huang, Jie Ma, Yanfei Chen, Liheng Wang, You Yang, and Qiong Liu. Sp-det: Leveraging saliency prediction for voxel-based 3d object detection in sparse point cloud. *IEEE Transactions on Multimedia*, 2023. doi:10.1109/TMM.2023.3304054.
- Xuyang Bai, Zeyu Hu, Xinge Zhu, Qingqiu Huang, Yilun Chen, Hongbo Fu, and Chiew-Lan Tai. Transfusion: Robust lidar-camera fusion for 3d object detection with transformers. In *Proceedings of the IEEE/CVF Conference on Computer Vision and Pattern Recognition*, pages 1090–1099, 2022.
- Nicolas Carion, Francisco Massa, Gabriel Synnaeve, Nicolas Usunier, Alexander Kirillov, and Sergey Zagoruyko. End-to-end object detection with transformers. In *European Conference on Computer Vision*, pages 213–229. Springer, 2020.
- Xiaozhi Chen, Huimin Ma, Ji Wan, Bo Li, and Tian Xia. Multi-view 3d object detection network for autonomous driving. In *Proceedings of the IEEE/CVF Conference on Computer Vision and Pattern Recognition*, pages 1907–1915, 2017.
- Angela Dai, Angel X. Chang, Manolis Savva, Maciej Halber, Thomas Funkhouser, and Matthias Nießner. Scannet: Richly-annotated 3d reconstructions of indoor scenes. In *Proceedings of the IEEE/CVF Conference on Computer Vision and Pattern Recognition*, pages 2432–2443, 2017.
- Jiajun Deng, Wengang Zhou, Yanyong Zhang, and Houqiang Li. From multi-view to hollow-3d: Hallucinated hollow-3d r-cnn for 3d object detection. *IEEE Transactions on Circuits and Systems for Video Technology*, 31(12):4722–4734, 2021.
- Zhuo Deng and Longin Jan Latecki. Amodal detection of 3d objects: Inferring 3d bounding boxes from 2d ones in rgb-depth images. In *Proceedings of the IEEE/CVF Conference on Computer Vision and Pattern Recognition*, pages 5762–5770, 2017.
- Baojie Fan, Kexin Zhang, and Jiandong Tian. Hcpvf: Hierarchical cascaded point-voxel fusion for 3d object detection. *IEEE Transactions on Circuits and Systems for Video Technology*, 2023. doi:10.1109/TCSVT.2023.3268849.
- Mingtao Feng, Syed Zulqarnain Gilani, Yaonan Wang, Liang Zhang, and Ajmal Mian. Relation graph network for 3d object detection in point clouds. *IEEE Transactions on Image Processing*, 30:92–107, 2020.
- Andreas Geiger, Philip Lenz, and Raquel Urtasun. Are we ready for autonomous driving? the kitti vision benchmark suite. In *Proceedings of the IEEE/CVF Conference on Computer Vision and Pattern Recognition*, pages 3354–3361, 2012.
- Benjamin Graham, Martin Engelcke, and Laurens Van Der Maaten. 3d semantic segmentation with submanifold sparse convolutional networks. In *Proceedings of the IEEE/CVF Conference on Computer Vision and Pattern Recognition*, pages 9224–9232, 2018.
- Noriaki Hirose, Shun Taguchi, Fei Xia, Roberto Martín-Martín, Kosuke Tahara, Masanori Ishigaki, and Silvio Savarese. Probabilistic visual navigation with bidirectional image prediction. In *IEEE/RSJ International Conference on Intelligent Robots and Systems*, pages 1539–1546. IEEE, 2021.
- Dinh-Cuong Hoang, Johannes A Stork, and Todor Stoyanov. Voting and attention-based pose relation learning for object pose estimation from 3d point clouds. *IEEE Robotics and Automation Letters*, 7(4):8980–8987, 2022.
- Ji Hou, Angela Dai, and Matthias Nießner. 3d-sis: 3d semantic instance segmentation of rgb-d scans. In *Proceedings of the IEEE/CVF Conference on Computer Vision and Pattern Recognition*, pages 4421–4430, 2019.
- Shan Jiayao, Sifan Zhou, Yubo Cui, and Zheng Fang. Real-time 3d single object tracking with transformer. *IEEE Transactions on Multimedia*, 25:2339–2353, 2023. doi:10.1109/TMM.2023.3146714.
- Abhijit Kundu, Yin Li, and James M Rehg. 3d-rnn: Instance-level 3d object reconstruction via render-and-compare. In *Proceedings of the IEEE Conference on Computer Vision and Pattern Recognition*, pages 3559–3568, 2018.
- Yangyan Li, Angela Dai, Leonidas Guibas, and Matthias Nießner. Database-assisted object retrieval for real-time 3d reconstruction. In *Computer Graphics Forum*, volume 34, pages 435–446, 2015.
- Yishi Li, Yuhao Zhang, and Rui Lai. Tinypillar: Tiny pillar-based network for 3d point cloud object detection at edge. *IEEE Transactions on Circuits and Systems for Video Technology*, 2023. doi:10.1109/TCSVT.2023.3297620.
- Or Litany, Tal Remez, Daniel Freedman, Lior Shapira, Alex Bronstein, and Ran Gal. Asist: automatic semantically invariant scene transformation. *Computer Vision and Image Understanding*, 157:284–299, 2017.
- Hao Liu, Yanni Ma, Qingyong Hu, and Yulan Guo. Centertube: Tracking multiple 3d objects with 4d tubelets in dynamic point clouds. *IEEE Transactions on Multimedia*, 2023. doi:10.1109/TMM.2023.3241548.

- [21] Zhanwen Liu, Juanru Cheng, Jin Fan, Shan Lin, Yang Wang, and Xiangmo Zhao. Multi-modal fusion based on depth adaptive mechanism for 3d object detection. *IEEE Transactions on Multimedia*, 2023. doi:10.1109/TMM.2023.3270638.
- [22] Zhe Liu, Tengting Huang, Bingling Li, Xiwu Chen, Xi Wang, and Xiang Bai. Epnnet++: Cascade bi-directional fusion for multi-modal 3d object detection. *IEEE Transactions on Pattern Analysis and Machine Intelligence*, 45(7):8324–8341, 2023.
- [23] Ishan Misra, Rohit Girdhar, and Armand Joulin. An end-to-end transformer model for 3d object detection. In *proceedings of the IEEE/CVF International Conference on Computer Vision*, pages 2906–2917, 2021.
- [24] Pushmeet Kohli Nathan Silberman, Derek Hoiem and Rob Fergus. Indoor segmentation and support inference from rgbd images. In *Proceedings of the European Conference on Computer Vision*, 2012.
- [25] Ramanpreet Singh Pahwa, Jiangbo Lu, Nianjuan Jiang, Tian Tsong Ng, and Minh N Do. Locating 3d object proposals: A depth-based online approach. *IEEE Transactions on Circuits and Systems for Video Technology*, 28(3):626–639, 2016.
- [26] Anshul Paigwar, David Sierra-Gonzalez, Özgür Ercent, and Christian Laugier. Frustum-pointpillars: A multi-stage approach for 3d object detection using rgb camera and lidar. In *Proceedings of the IEEE/CVF International Conference on Computer Vision*, pages 2926–2933, 2021.
- [27] Jin-Chun Piao and Shin-Dug Kim. Real-time visual-inertial slam based on adaptive keyframe selection for mobile ar applications. *IEEE Transactions on Multimedia*, 21(11):2827–2836, 2019.
- [28] Charles R Qi, Xinlei Chen, Or Litany, and Leonidas J Guibas. Imvotenet: Boosting 3d object detection in point clouds with image votes. In *Proceedings of the IEEE/CVF Conference on Computer Vision and Pattern Recognition*, pages 4404–4413, 2020.
- [29] Charles R. Qi, Or Litany, Kaiming He, and Leonidas J. Guibas. Deep hough voting for 3d object detection in point clouds. In *proceedings of the IEEE/CVF International Conference on Computer Vision*, pages 9277–9286, 2019.
- [30] Charles R Qi, Wei Liu, Chenxia Wu, Hao Su, and Leonidas J Guibas. Frustum pointnets for 3d object detection from rgb-d data. In *Proceedings of the IEEE/CVF Conference on Computer Vision and Pattern Recognition*, pages 918–927, 2018.
- [31] Charles R Qi, Hao Su, Kaichun Mo, and Leonidas J Guibas. Pointnet: Deep learning on point sets for 3d classification and segmentation. In *Proceedings of the IEEE Conference on Computer Vision and Pattern Recognition*, pages 652–660, 2017.
- [32] Charles R Qi, Li Yi, Hao Su, and Leonidas J Guibas. Pointnet++: Deep hierarchical feature learning on point sets in a metric space. In *Advances in Neural Information Processing Systems*, pages 5099–5108, 2017.
- [33] Colin Rennie, Rahul Shome, Kostas E Bekris, and Alberto F De Souza. A dataset for improved rgbd-based object detection and pose estimation for warehouse pick-and-place. *IEEE Robotics and Automation Letters*, 1(2):1179–1185, 2016.
- [34] Danila Rukhovich, Anna Vorontsova, and Anton Konushin. Imvoxelnet: Image to voxels projection for monocular and multi-view general-purpose 3d object detection. In *Proceedings of the IEEE/CVF Winter Conference on Applications of Computer Vision*, pages 2397–2406, 2022.
- [35] Shaoshuai Shi, Zhe Wang, Jianping Shi, Xiaogang Wang, and Hongsheng Li. From points to parts: 3d object detection from point cloud with part-aware and part-aggregation network. *IEEE Transactions on Pattern Analysis and Machine Intelligence*, 43(8):2647–2664, 2021.
- [36] Kiwoo Shin, Youngwook Paul Kwon, and Masayoshi Tomizuka. Roar-net: A robust 3d object detection based on region approximation refinement. In *IEEE Intelligent Vehicles Symposium*, pages 2510–2515. IEEE, 2019.
- [37] Shuran Song, Samuel P Lichtenberg, and Jianxiong Xiao. Sun rgb-d: A rgb-d scene understanding benchmark suite. In *Proceedings of the IEEE/CVF Conference on Computer Vision and Pattern Recognition*, pages 567–576, 2015.
- [38] Shuran Song and Jianxiong Xiao. Sliding shapes for 3d object detection in depth images. In *Proceedings of the European Conference on Computer Vision*, pages 634–651, 2014.
- [39] Shuran Song and Jianxiong Xiao. Deep sliding shapes for amodal 3d object detection in rgb-d images. In *Proceedings of the IEEE/CVF Conference on Computer Vision and Pattern Recognition*, pages 808–816, 2016.
- [40] Matthew Tancik, Pratul Srinivasan, Ben Mildenhall, Sara Fridovich-Keil, Nithin Raghavan, Utkarsh Singhal, Ravi Ramamoorthi, Jonathan Barron, and Ren Ng. Fourier features let networks learn high frequency functions in low dimensional domains. *Advances in Neural Information Processing Systems*, 33:7537–7547, 2020.
- [41] Haotian Tang, Zhijian Liu, Shengyu Zhao, Yujun Lin, Ji Lin, Hanrui Wang, and Song Han. Searching efficient 3d architectures with sparse point-voxel convolution. In *Proceedings of the European Conference on Computer Vision*, 2020.
- [42] Guofeng Tong, Zheng Li, Hao Peng, and Yaqi Wang. Multi-source features fusion single stage 3d object detection with transformer. *IEEE Robotics and Automation Letters*, 8(4):2062–2069, 2023.
- [43] Ashish Vaswani, Noam Shazeer, Niki Parmar, Jakob Uszkoreit, Llion Jones, Aidan N Gomez, Łukasz Kaiser, and Illia Polosukhin. Attention is all you need. In *Advances in Neural Information Processing Systems*, pages 5998–6008, 2017.
- [44] Sourabh Vora, Alex H Lang, Bassam Helou, and Oscar Beijbom. Point-painting: Sequential fusion for 3d object detection. In *Proceedings of the IEEE/CVF Conference on Computer Vision and Pattern Recognition*, pages 4604–4612, 2020.
- [45] Deming Wang, Guangliang Zhou, Yi Yan, Huiyi Chen, and Qijun Chen. Geopose: Dense reconstruction guided 6d object pose estimation with geometric consistency. *IEEE Transactions on Multimedia*, 24:4394–4408, 2021.
- [46] Jian Wang, Fan Li, Xuchong Zhang, and Hongbin Sun. Adversarial obstacle generation against lidar-based 3d object detection. *IEEE Transactions on Multimedia*, 2023. doi:10.1109/TMM.2023.3302018.
- [47] Shuhua Wang, Ke Lu, Jian Xue, and Yang Zhao. Da-net: Density-aware 3d object detection network for point clouds. *IEEE Transactions on Multimedia*, 2023. doi:10.1109/TMM.2023.3245359.
- [48] Zhixin Wang and Kui Jia. Frustum convnet: Sliding frustums to aggregate local point-wise features for amodal 3d object detection. In *IEEE/RSJ International Conference on Intelligent Robots and Systems*, pages 1742–1749. IEEE, 2019.
- [49] Fei Xia, William B Shen, Chengshu Li, Priya Kasimbeg, Micael Edmond Tchampi, Alexander Toshev, Roberto Martín-Martín, and Silvio Savarese. Interactive gibbon benchmark: A benchmark for interactive navigation in cluttered environments. *IEEE Robotics and Automation Letters*, 5(2):713–720, 2020.
- [50] Bangqian Xie, Liang Yang, Ailin Wei, Xiaoxiong Weng, and Bing Li. Mutrans: Multiple transformers for fusing feature pyramid on 2d and 3d object detection. *IEEE Transactions on Image Processing*, 32:4407–4415, 2023. doi:10.1109/TIP.2023.3299190.
- [51] Tao Xie, Li Wang, Ke Wang, Ruifeng Li, Xinyu Zhang, Haoming Zhang, Linqi Yang, Huaping Liu, and Jun Li. Farp-net: Local-global feature aggregation and relation-aware proposals for 3d object detection. *IEEE Transactions on Multimedia*, 2023. doi:10.1109/TMM.2023.3275366.
- [52] Danfei Xu, Dragomir Anguelov, and Ashesh Jain. Pointfusion: Deep sensor fusion for 3d bounding box estimation. In *Proceedings of the IEEE/CVF Conference on Computer Vision and Pattern Recognition*, pages 244–253, 2018.
- [53] Shaoqing Xu, Dingfu Zhou, Jin Fang, Junbo Yin, Zhou Bin, and Liangjun Zhang. Fusionpainting: Multimodal fusion with adaptive attention for 3d object detection. In *IEEE International Intelligent Transportation Systems Conference*, pages 3047–3054. IEEE, 2021.
- [54] Tong Xue, Abdallah El Ali, Tianyi Zhang, Gangyi Ding, and Pablo Cesar. Ceap-360vr: A continuous physiological and behavioral emotion annotation dataset for 360 vr videos. *IEEE Transactions on Multimedia*, 25:243–255, 2023. doi:10.1109/TMM.2021.3124080.
- [55] Yan Yan, Yuxing Mao, and Bo Li. Second: Sparsely embedded convolutional detection. *Sensors*, 18(10):3337, 2018.
- [56] Tianwei Yin, Xingyi Zhou, and Philipp Krähenbühl. Multimodal virtual point 3d detection. *Advances in Neural Information Processing Systems*, 34:16494–16507, 2021.
- [57] Haitao Zeng, Xinhang Song, and Shuqiang Jiang. Multi-object navigation using potential target position policy function. *IEEE Transactions on Image Processing*, 2023. doi:10.1109/TIP.2023.3263110.
- [58] Zaiwei Zhang, Rohit Girdhar, Armand Joulin, and Ishan Misra. Self-supervised pretraining of 3d features on any point-cloud. In *Proceedings of the IEEE/CVF International Conference on Computer Vision*, pages 10252–10263, 2021.
- [59] Kun Zhao, Lingfei Ma, Yu Meng, Li Liu, Junbo Wang, José Marcato Junior, Wesley Nunes Gonçalves, and Jonathan Li. 3d vehicle detection using multi-level fusion from point clouds and images. *IEEE Transactions on Intelligent Transportation Systems*, 23(9):15146–15154, 2022.
- [60] Lichen Zhao, Jinyang Guo, Dong Xu, and Lu Sheng. Transformer3d-det: Improving 3d object detection by vote refinement. *IEEE Transactions on Circuits and Systems for Video Technology*, 31(12):4735–4746, 2021.
- [61] Zheyuan Zhou, Liang Du, Xiaoqing Ye, Zhikang Zou, Xiao Tan, Li Zhang, Xiangyang Xue, and Jianfeng Feng. Sgm3d: stereo guided monocular 3d object detection. *IEEE Robotics and Automation Letters*, 7(4):10478–10485, 2022.
- [62] Hanqi Zhu, Jiajun Deng, Yu Zhang, Jianmin Ji, Qiuyu Mao, Houqiang Li, and Yanyong Zhang. Vpfnnet: Improving 3d object detection with virtual point based lidar and stereo data fusion. *IEEE Transactions on Multimedia*, pages 1–14, 2022. doi:10.1109/TMM.2022.3189778.